The Astrophysical Journal, 711:641–654, 2010 March 10 doi:10.1088/0004-637X/711/2/641

THE COLLIMATION AND ENERGETICS OF THE BRIGHTEST *SWIFT* GAMMA-RAY BURSTS

S. B. Cenko[1], D. A. Frail[2], F. A. Harrison[3], S. R. Kulkarni[4], E. Nakar[5], P. C. Chandra[6], N. R. Butler[1], D. B. Fox[7], A. Gal-Yam[8], M. M. Kasliwal[4], J. Kelemen[9], D.-S. Moon[10], E. O. Ofek[4,21], P. A. Price[11], A. Rau[4,12], A. M. Soderberg[13,22], H. I. Teplitz[14], M. W. Werner[15], D. C.-J. Bock[16], J. S. Bloom[1], D. A. Starr[1,17], A. V. Filippenko[1], R. A. Chevalier[18], N. Gehrels[19], J. N. Nousek[7], and T. Piran[20]

[1] Department of Astronomy, University of California, Berkeley, CA 94720-3411, USA
[2] National Radio Astronomy Observatory, P.O. Box 0, 1003 Lopezville Road, Socorro, NM 87801, USA
[3] Space Radiation Laboratory, California Institute of Technology, MS 249-17, Pasadena, CA 91125, USA
[4] Department of Astronomy, California Institute of Technology, MS 249-17, Pasadena, CA 91125, USA
[5] Raymond and Beverly Sackler School of Physics & Astronomy, Tel Aviv University, Tel Aviv 69978, Israel
[6] Department of Physics, Royal Military College of Canada, Kingston, ON, Canada
[7] Department of Astronomy & Astrophysics, 525 Davey Laboratory, Pennsylvania State University, University Park, PA 16802, USA
[8] Benoziyo Center for Astrophysics, Weizmann Institute of Science, 76100 Rehovot, Israel
[9] Konkoly Observatory, H-1525, Box 67, Budapest, Hungary
[10] Department of Astronomy and Astrophysics, University of Toronto, Toronto, ON M5S 3H4, Canada
[11] Institute for Astronomy, University of Hawaii, 2680 Woodlawn Drive, Honolulu, HI 96822, USA
[12] Max-Planck Institute for Extra-Terrestrial Physics, Giessenbachstr. 1, 85748 Garching, Germany
[13] Harvard-Smithsonian Center for Astrophysics, 60 Garden Street, Cambridge, MA 02138, USA
[14] Spitzer Science Center, California Institute of Technology, Pasadena, CA 91125, USA
[15] Jet Propulsion Laboratory, California Institute of Technology, 4800 Oak Grove Drive, Pasadena, CA 91109, USA
[16] Combined Array for Research in Millimeter-wave Astronomy, P.O. Box 968, Big Pine, CA 93513, USA
[17] Las Cumbres Observatory Global Telescope Network, Inc., 6740 Corona Dr., Suite 102, Santa Barbara, CA 93117, USA
[18] Department of Astronomy, University of Virgina, P.O. Box 400325, Charlottesville, VA 22904, USA
[19] Astrophysics Science Division, Code 660.1, NASA/Goddard Space Flight Center, Greenbelt, MD 20770, USA
[20] The Racah Institute of Physics, Hebrew University, Jerusalem 91904, Israel
Received 2009 May 5; accepted 2010 January 19; published 2010 February 17

ABSTRACT

Long-duration gamma-ray bursts (GRBs) are widely believed to be highly collimated explosions (bipolar conical outflows with half-opening angle $\theta \approx 1^\circ$–10°). As a result of this beaming factor, the true energy release from a GRB is usually several orders of magnitude smaller than the observed isotropic value. Measuring this opening angle, typically inferred from an achromatic steepening in the afterglow light curve (a "jet" break), has proven exceedingly difficult in the *Swift* era. Here, we undertake a study of five of the brightest (in terms of the isotropic prompt γ-ray energy release, $E_{\gamma,\rm iso}$) GRBs in the *Swift* era to search for jet breaks and hence constrain the collimation-corrected energy release. We present multi-wavelength (radio through X-ray) observations of GRBs 050820A, 060418, and 080319B, and construct afterglow models to extract the opening angle and beaming-corrected energy release for all three events. Together with results from previous analyses of GRBs 050904 and 070125, we find evidence for an achromatic jet break in all five events, strongly supporting the canonical picture of GRBs as collimated explosions. The most natural explanation for the lack of observed jet breaks from most *Swift* GRBs is therefore selection effects. However, the opening angles for the events in our sample are larger than would be expected if all GRBs had a canonical energy release of $\sim 10^{51}$ erg. The total energy release we measure for the "hyper-energetic" ($E_{\rm tot} \gtrsim 10^{52}$ erg) events in our sample is large enough to start challenging models with a magnetar as the compact central remnant.

Key words: gamma-ray burst: general – X-rays: individual (GRB 050820A, GRB 050904, GRB 060418, GRB 070125, GRB 080319B)

Online-only material: color figures

1. INTRODUCTION

Accurate calorimetry is fundamental to understanding any astrophysical phenomenon. In the case of long-duration gamma-ray bursts (GRBs),[23] three measurements are required for an accounting of the total relativistic[24] energy release: (1) $E_{\gamma,\rm iso}$, the isotropic energy release in the prompt γ-ray emission, which is inferred from the γ-ray fluence measured by the detecting satellite and the associated afterglow or host redshift; (2) θ, the opening angle of the beamed emission, which is inferred from the detection of a characteristic achromatic steepening in the afterglow light curve (i.e., a "jet" break; Rhoads 1999; Sari et al. 1999); and (3) $E_{\rm KE}$, the kinetic energy of the shock powering the afterglow emission, which can be inferred either via broadband afterglow modeling (e.g., Panaitescu & Kumar 2002; Yost et al. 2003) or, more accurately, from late-time radio calorimetry in the non-relativistic phase (e.g., Berger et al. 2004; Frail et al. 2005; van der Horst et al. 2008).

Compilations of such measurements for the first GRB afterglows suggested that the collimation-corrected energy release, either from the prompt γ-rays (E_γ) or powering the afterglow

[21] Einstein Fellow.
[22] Hubble Fellow.
[23] Throughout this work, we use the term "long-duration" GRBs to refer to those events that arise from the core collapse of a massive star (Woosley 1993; Woosley & Bloom 2006), despite the fact that duration alone is not sufficient to distinguish from those GRBs associated with an older stellar population (e.g., Donaghy et al. 2006; Zhang et al. 2009).
[24] We neglect contributions from slower moving material (i.e., SN emission) as well as non-electromagnetic emission (neutrinos, gravitational radiation, etc.).

($E_{\rm KE}$), was tightly clustered around $\sim 10^{51}$ erg (Frail et al. 2001; Berger et al. 2003a; Bloom et al. 2003). This result helped to establish the connection between GRBs and massive stars, as core-collapse supernovae (SNe) result in a comparable output of kinetic energy. It further motivated efforts to utilize GRBs as standardizable candles to constrain the cosmological model of the universe (e.g., Dai et al. 2004; Firmani et al. 2006; Schaefer 2007), much as has been done for Type Ia SNe (Riess et al. 1998; Perlmutter et al. 1999; see, e.g., Filippenko 2005 for a review).

It was soon realized, however, that the most nearby (redshift $z \lesssim 0.1$) GRBs were several orders of magnitude less energetic than the typical GRB at $z \gtrsim 1$ (Bloom et al. 2003; Soderberg et al. 2004). Furthermore, these underluminous events appear to be significantly more common (in terms of volumetric rate) than their cosmological brethren (Soderberg et al. 2006; Cobb et al. 2006; Guetta & Valle 2007). Though the reason for this dichotomy remains a mystery, it suggests that perhaps long-duration GRBs are a more diverse population than originally envisioned.

The launch of the *Swift* satellite (Gehrels et al. 2004) in 2004 November heralded a potential revolution in the study of GRB energetics. With its unique combination of sensitivity ($\sim$100 GRB localizations yr^{-1}, an order of magnitude improvement over previous satellites) and precise localization capabilities ($\sim 3'$ positions arrive only seconds after the GRB trigger, with $\sim 3''$ positions delivered minutes later), *Swift* promised to deliver a tremendous increase in the number of events suitable for detailed studies of energetics.

Furthermore, the onboard X-ray telescope (XRT; Burrows et al. 2005a) has provided the first detailed look at X-ray afterglow evolution. Before the launch of *Swift*, opening angles were typically inferred from the optical and occasionally from radio bandpasses. X-ray afterglows, particularly at early times, were a relatively poorly sampled phase space. The additional leverage provided by the X-ray regime promised to greatly simplify the task of distinguishing jet breaks from other predicted spectral features in afterglow light curves due to the achromatic nature of this hydrodynamical transition.

Despite these advances, measuring bolometric fluences of *Swift* events has proven to be a challenging task. First, the limited bandpass (15–150 keV) of the *Swift* Burst Alert Telescope (BAT; Barthelmy et al. 2005) captures only a fraction of the traditional γ-ray regime. As shown by Figure 1, the uncertainties associated with *Swift* $E_{\gamma,\rm iso}$ measurements are significantly larger than in the pre-*Swift* sample, due to the difficulty in extrapolating to the 1–10^4 keV (rest-frame) bolometric bandpass. We note that the *Swift* measurements shown in Figure 1 incorporate a Bayesian prior on the spectral peak energy ($E_{\rm p}$) based on the $E_{\rm p}$ distribution measured by the BATSE instrument (see Butler et al. 2007 for details). We caution that such an approach may introduce subtle biases into the *Swift* $E_{\rm p}$ (and hence $E_{\gamma,\rm iso}$) measurements due to the different bandpasses and responses of the two detectors.[25] However, without this constraint the $E_{\gamma,\rm iso}$ measurements would have even larger uncertainties.

Second, the detailed X-ray light curves provided by the *Swift* XRT have revealed a central engine capable of injecting energy into the forward shock at late times ($t \gg \Delta t_{\rm GRB}$), either as short-lived X-ray flares that can contain a comparable amount of energy to E_γ (Burrows et al. 2005b), or as extended periods of shallow decay (the so-called plateau phases) inconsistent with standard afterglow models (Fan & Piran 2006; Nousek et al. 2006; Zhang et al. 2006). While alternative interpretations for both phenomena exist, these discoveries suggest that our simplistic adiabatic picture of afterglow evolution may need to be revised.

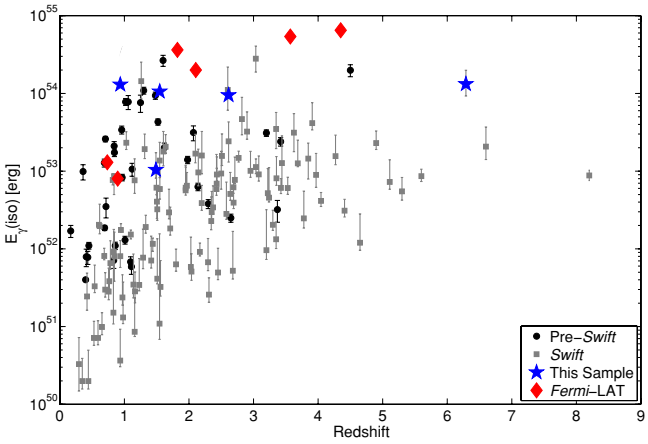

Figure 1. Isotropic prompt γ-ray energy release ($E_{\gamma,\rm iso}$) of GRBs with measured redshift. All prompt energy releases have been transformed to the rest-frame 1 keV to 10 MeV bandpass. The increased sensitivity of the *Swift* BAT results in a population with lower values of $E_{\gamma,\rm iso}$ and larger redshifts. It is not surprising, then, that typical *Swift* events should have large (or even isotropic) opening angles, making jet-break measurements quite difficult (Perna et al. 2003). In this work, we focus on those events in the *Swift* sample with the largest values of $E_{\gamma,\rm iso}$. References: pre-*Swift*: Amati (2006); *Swift*: Butler et al. (2007); *Fermi*-LAT: Greiner et al. (2009); Golenetskii et al. (2009b); Rau et al. (2009); Abdo et al. (2009a); Golenetskii et al. (2009a); Rau (2009).

(A color version of this figure is available in the online journal.)

Most importantly, surprisingly few *Swift* afterglows have shown the characteristic achromatic steepening associated with a collimated outflow. Several groups have conducted a comprehensive analysis of a large sample of X-ray (Panaitescu 2007; Kocevski & Butler 2008; Racusin et al. 2009) and/or optical (Liang et al. 2008) light curves, finding that at most only a small fraction exhibit clear evidence for collimation. Without these collimation corrections, the true energy release from *Swift* events has remained highly uncertain (e.g., Kocevski & Butler 2008; Racusin et al. 2009).

Here, we take a different approach. To begin with, we focus only on those *Swift* events with the largest values of $E_{\gamma,\rm iso}$ (Figure 1). In the framework of a canonical GRB energy release, these events should have the smallest opening angles, thereby easing to some extent the observational bias against late-time jet breaks. Alternatively, if isotropic, these extreme events would place the strongest constraints on the mechanism powering these explosions. Such high-fluence events are also more likely to be detected by other γ-ray satellites, providing additional coverage in the traditional γ-ray bandpass and thereby better constraining the prompt γ-ray energy release.

In addition, we only consider GRB afterglows with broadband (X-ray, optical, *and* radio) coverage extending out to late times ($t \gtrsim 1$ month). The radio bandpass is particularly sensitive to wide-angle jets, as the synchrotron peak frequency typically does not reach the radio bandpass until days or even weeks after the burst, when the X-ray and optical bands may be too faint to detect a jet break. Well-sampled, broadband light curves ensure accurate constraints on both the opening angle and the kinetic energy powering the afterglow (e.g., Curran et al. 2007).

[25] Our approach of selecting only the brightest events largely circumvents this issue, as all events in our sample except GRB 050904 were detected by additional satellites with wider high-energy bandpasses.

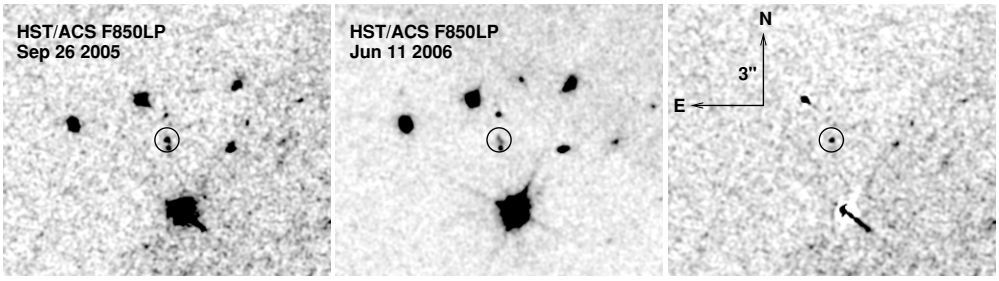

Figure 2. *HST* imaging of GRB 050820A. Left: an $F850LP$ ACS image taken on 2005 September 26. Center: the same field in an image obtained on 2006 June 11. Right: a digital subtraction of the two images, revealing the residual afterglow emission. The host-galaxy contribution to the afterglow flux at the time of the 2005 September 26 image is significant (∼35%). All images are oriented with north up and east to the left, and have been smoothed with a three-pixel Gaussian filter.

Given these constraints, we include five events in our *Swift* sample: GRBs 050820A, 050904, 060418, 070125, and 080319B. This sample is not meant to be representative of the *Swift* population as a whole. Nor, for that matter, have we included *all* of the *Swift* events with large $E_{\gamma,\rm iso}$ values, as most lack the radio and late-time optical coverage necessary for afterglow modeling (e.g., GRB 061007; Schady et al. 2007). Instead, we argue that great insight, in particular with regard to progenitor models, can come from studies of even a small number of events at the extreme (see, e.g., GRB 080721; Starling et al. 2009).

This work is organized as follows. In Section 2, we present our observations of the afterglows of GRB 050820A, GRB 060418, and GRB 080319B. We then construct broadband afterglow models to extract the opening angle and afterglow energy for each one in Section 3. To complete our sample, we include analogous results from previous broadband modeling of GRB 050904 (Frail et al. 2006) and GRB 070125 (Chandra et al. 2008). We compare the total energy release from these five events with the pre-*Swift* sample in Section 4, and conclude in Section 5 with a discussion of the future of GRB energetics studies.

Throughout this work, we adopt a standard ΛCDM cosmology with $H_0 = 71$ km s^{-1} Mpc^{-1}, $\Omega_{\rm m} = 0.27$, and $\Omega_\Lambda = 1 - \Omega_{\rm m} = 0.73$ (Spergel et al. 2007). We define the flux density power-law temporal and spectral decay indices α and β as $f_\nu \propto t^{-\alpha}\nu^{-\beta}$ (e.g., Sari et al. 1998). All errors quoted are 1σ (68%) confidence intervals unless otherwise noted.

2. OBSERVATIONS AND DATA REDUCTION

2.1. GRB 050820A

GRB 050820A was remarkable in two respects. First, the *Swift* BAT triggered on a faint γ-ray precursor nearly 4 minutes before the bulk of the prompt emission, enabling contemporaneous γ-ray, X-ray, and optical coverage during the GRB itself. Both the X-ray and (to a lesser extent) the optical emission abruptly brightened in concert with the onset of the GRB, suggesting a common origin (Vestrand et al. 2006).

The prompt emission was observed by the Konus/*Wind* instrument, providing spectral coverage from 20 keV to 1 MeV (Cenko et al. 2006b). Extrapolating the observed spectrum to a rest-frame bandpass of 1–10^4 MeV, we find a fluence of $(6.1^{+1.9}_{-0.9}) \times 10^{-5}$ erg cm^{-2}. At $z = 2.615$ (Prochaska et al. 2007), the total isotropic prompt energy release in this bandpass was $E_{\gamma,\rm iso} = (9.7^{+3.1}_{-1.4}) \times 10^{53}$ erg.

In addition, the X-ray and particularly optical afterglow emission from GRB 050820A was quite bright, allowing the decay to be traced out to late times. The majority of our observations of GRB 050820A were presented by Cenko et al. (2006b). We reported the detection of a likely jet break at $t_{\rm j} = 18 \pm 2$ days based on late-time *Hubble Space Telescope* (*HST*) observations, later than nearly all previously detected jet breaks in the optical bandpass (Zeh et al. 2006).

Here, we supplement this already rich data set with additional late-time X-ray and optical imaging. *Swift* XRT data were taken from the online compilation of N. Butler.[26] These detections extend the X-ray coverage out to $t \approx 46$ days, well past the previously claimed jet-break time.

We have also obtained optical imaging of the host galaxy of GRB 050820A using the Wide Field Channel (WFC) of the Advanced Camera for Surveys (ACS) on *HST* (Figure 2). Under program GO-10551 (PI: Kulkarni), we obtained a total of 2238 s of exposure time in the $F625W$ (Sloan r') filter, 4404 s of exposure time in the $F775W$ (Sloan i') filter, and 14280 s of exposure time in the $F850LP$ (Sloan z') filter beginning on 2006 June 5 (UT dates are used throughout this paper). We processed the data using the `multidrizzle` routine (Fruchter & Hook 2002) in the `stsdas` IRAF[27] package. We used `pixfrac` = 0.8 and `pixscale` = 1.0 for the drizzling procedure, resulting in a scale of 0.″05 pixel^{-1}. Following the recipe for point-source[28] photometry from Sirianni et al. (2005), we measure the following (AB) magnitudes: $F625W = 26.04 \pm 0.13$, $F775W = 26.09 \pm 0.11$, and $F850LP = 25.91 \pm 0.11$ (including a correction for the small amount of Galactic extinction: $E(B-V) = 0.044$ mag; Schlegel et al. 1998). These results are consistent with, although slightly brighter than, the values reported by Chen et al. (2009).

The detection of the host galaxy allows us to subtract its contribution from the afterglow measured at $t \approx 36$ days with ACS. As can be seen from Figure 2, the host contribution at this epoch is significant and will affect the jet-break time measured in Section 3.

The combined X-ray, optical, and radio light curves of GRB 050820A are shown in Figure 3.

2.2. GRB 060418

GRB 060418 was detected by the *Swift* BAT at 03:06:08 on 2006 April 18 (Falcone et al. 2006a). The γ-ray light curve shows three overlapping peaks with a total duration $t_{90} = 52 \pm 1$ s (Cummings et al. 2006). GRB 060418 was also bright enough to be detected with Konus/*Wind*, but no uncertainties were provided on the derived spectral parameters (Golenetskii

[26] http://astro.berkeley.edu/∼nat/swift; see Butler & Kocevski (2007) for details.

[27] IRAF is distributed by the National Optical Astronomy Observatory, which is operated by the Association for Research in Astronomy, Inc., under cooperative agreement with the National Science Foundation (NSF).

[28] The host galaxy is only marginally extended in the *HST* images.

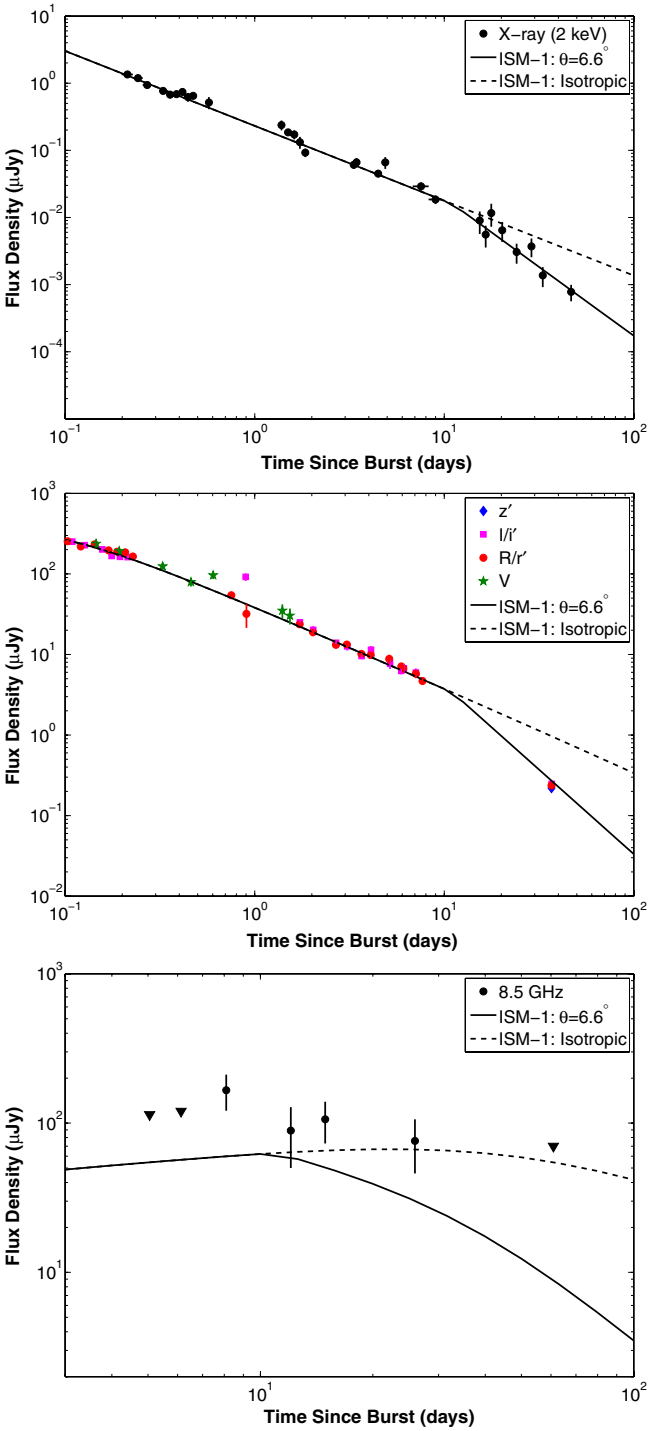

Figure 3. X-ray (top panel), optical (middle panel), and radio (bottom panel) light curves of GRB 050820A. Radio observations at $t < 5$ days are left out of the model, as the emission at this time is likely dominated by the reverse shock (Cenko et al. 2006b). The preferred model (ISM-1; Table 4) is plotted as a solid line, while the identical model for an isotropic explosion is shown as a dashed line. The optical data have been scaled by the model flux to match the R_C-band. Both the X-ray and optical bandpasses show a clear break at $t \approx 10$ days. The radio is not sufficient to distinguish between an isotropic and a collimated outflow.

(A color version of this figure is available in the online journal.)

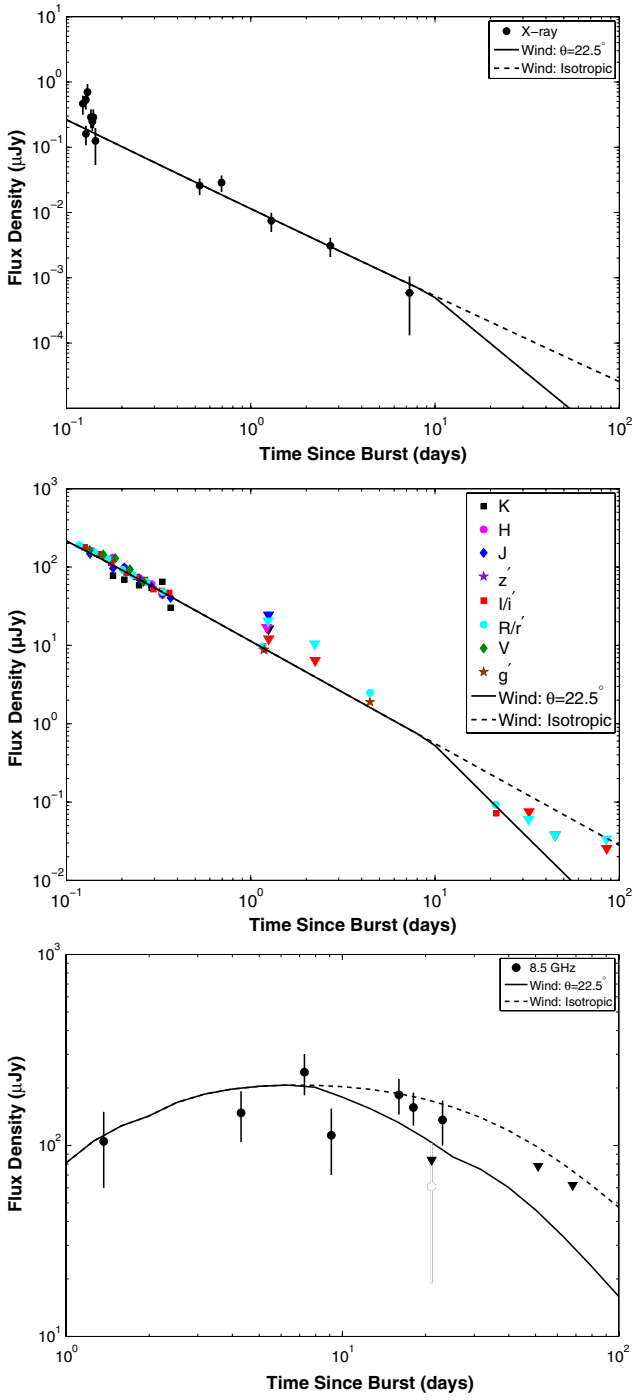

Figure 4. X-ray (top panel), optical (middle panel), and radio (bottom panel) light curves of GRB 060418. The preferred model (Wind—Table 5) is plotted as a solid line, while the identical model for an isotropic explosion is shown as a dashed line. The optical data have been scaled by the model flux to match the R_C-band. The optical shows a clear break at $t \approx 10$ days, which is also favored in the radio. The X-ray afterglow is too faint to be detected at this time.

(A color version of this figure is available in the online journal.)

et al. 2006). We therefore use the rest-frame 1–10^4 keV fluence derived from the *Swift*-BAT by Butler et al. (2007). At $z = 1.49$ (Prochaska et al. 2007), the total isotropic prompt energy release from GRB 060418 was $E_{\gamma,\rm iso} = (1.0^{+0.7}_{-0.2}) \times 10^{53}$ erg, consistent with the value inferred from Konus/*Wind*.

The XRT promptly slewed to the burst location and detected a fading X-ray counterpart at $\alpha = 15^{\rm h}45^{\rm m}42\overset{\rm s}{.}8$, $\delta = -03^\circ38'26\overset{''}{.}1$ (J2000.0; $5\overset{''}{.}8$ error radius; Falcone et al. 2006a). Like many *Swift* X-ray afterglows, the light curve exhibits a bright flare at $t \approx 128$ s superposed on a power-law decay (Falcone et al. 2006b). In Figure 4, we plot the X-ray light curve evolution for $t > 0.1$ days, obtained from the online catalog of N. Butler.

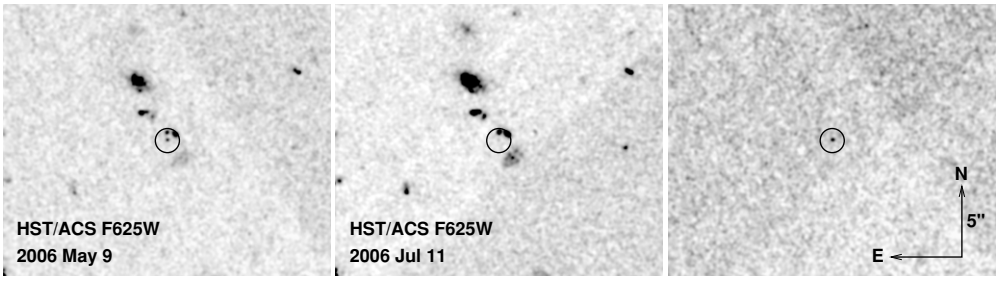

Figure 5. *HST* imaging of GRB 060418. Left: an *F625W* ACS image taken on 2006 May 9. Center: the same field in an image obtained on 2006 July 11. Right: a digital subtraction of the two images, revealing the residual afterglow emission. There is no sign of any host-galaxy emission coincident with the afterglow; however, the photometry is complicated by contamination from several nearby sources (which may be related to the host galaxy; Pollack et al. 2009). All images are oriented with north up and east to the left, and have been smoothed with a three-pixel Gaussian filter.

The automated Palomar 60 inch (1.5 m) telescope (P60; Cenko et al. 2006a) began observing the afterglow of GRB 060418 in the V_C, R_C, and i' filters beginning 2.7 hr after the burst (when the source became visible at Palomar Observatory). P60 data were reduced in the IRAF environment using our custom real-time reduction pipeline (Cenko et al. 2006a). Where necessary, co-addition was performed using Swarp.[29] Afterglow magnitudes were calculated with aperture photometry using an inclusion radius roughly matched to the full width at half-maximum (FWHM) intensity of the stellar point-spread function (PSF). Photometric calibration was performed relative to the calibration files provided by A. Henden,[30] resulting in root-mean-square (rms) variations of $\lesssim$0.05 mag in all filters. Photometric and instrumental errors have been added in quadrature to obtain the results presented in Table 1.

Additional optical imaging was obtained with two large ground-based facilities to supplement the P60 light curves at late times: the Large Format Camera (LFC) mounted on the 200 inch (5.1 m) Palomar Hale telescope, and the Low Resolution Imaging Spectrometer (LRIS; Oke et al. 1995) mounted on the 10 m Keck I telescope. All data were reduced in a manner similar to the P60 images using standard IRAF routines.

Late-time observations of GRB 060418 were obtained with the WFC channel of the ACS on *HST* (GO-10551; PI: Kulkarni). The images were processed in an identical manner to that described in Section 2.1. There is no evidence for host-galaxy emission directly coincident with the afterglow location. However, several nearby sources, which may be related to the host galaxy (Pollack et al. 2009), may contaminate the afterglow photometry. The results of these observations are shown in Table 1 and Figure 5.

The 1.3 m Peters Automated Infrared Telescope (PAIRITEL; Bloom et al. 2006) began observing the afterglow of GRB 060418 at 5:25:34 on 2006 April 18. Full details of the PAIRITEL observations are presented by Pollack et al. (2009). Here, we present the full multi-color PAIRITEL light curve of GRB 060418, derived using aperture photometry and calibrated with respect to the Two Micron All Sky Survey (2MASS; Skrutskie et al. 2006). The results of our analysis are shown in Table 1.

Finally, we began observations of the fading optical counterpart of GRB 060418 with the Very Large Array (VLA)[31] approximately 1 d after the burst. The results of this and subsequent monitoring for 68 days after the burst are summarized in Table 2. For the majority of the observations, the antennas were in the "A" configuration; the sole exceptions are the data points on 2006 June 8 ("BnA") and 2006 June 25 ("B"). All observations were reduced with the Astronomical Image Processing Software (AIPS) in the standard manner.

The resulting X-ray, optical, and radio light curves of GRB 060418 are shown in Figure 4.

2.3. GRB 080319B

GRB 080319B, or the "naked-eye burst," has been discussed extensively in the literature. The most remarkable aspect of this unique event was the bright optical flash (peak optical magnitude of 5.3; Racusin et al. 2008) that accompanied the prompt γ-ray emission. Because of the temporal coincidence, the contemporaneous γ-ray and optical emission are believed to derive from the same physical region, with the observed γ-rays being generated by Compton scattering from the same relativistic electrons that cause the optical flash (Racusin et al. 2008; Kumar & Panaitescu 2008).

The best constraints on the prompt emission come from the Konus/*Wind* satellite. The measured (20 keV–7 MeV) fluence does not change appreciably when converting to the standard bandpass. The resulting isotropic prompt energy release at $z = 0.937$ (Racusin et al. 2008; D'Elia et al. 2009) is $E_{\gamma,\rm iso} = (1.44 \pm 0.03) \times 10^{54}$ erg (Racusin et al. 2008).

For our modeling of GRB 080319B, we draw on the rich data sets of Racusin et al. (2008), Bloom et al. (2009), Tanvir et al. (2008), and Cenko et al. (2009). To supplement these results, we obtained target-of-opportunity observations of the afterglow of GRB 080319B in peak-up imaging mode (i.e., with the blue 15.8 μm filter) of the Infrared Spectrograph (IRS) on the *Spitzer Space Telescope* through a Director's Discretionary Time proposal. We obtained 60 dithered pointings, each consisting of two 30 s cycles, beginning at 2008 March 21.81 ($\sim$2.55 d after the burst). We clearly detect the afterglow at this time with a flux density of 35.7 ± 3.9 μJy (Teplitz et al. 2008). A second set of observations was obtained beginning at 2008 March 29.89, this time using 120 pointings. No source was detected to a (1σ) limiting magnitude of 4.0 μJy. The results of these observations are summarized in Figure 6 and Table 3.

We also observed the location of GRB 080319B with the Combined Array for Research in Millimeter-wave Astronomy (CARMA) at 95 GHz on 2008 March 20 (mean time 11:30). The configuration and data reduction are identical to those described by Chandra et al. (2008). We report a nondetection at the optical afterglow position with a 2σ limit of 0.50 mJy (Bock et al. 2008).

[29] See http://terapix.iap.fr/soft/swarp
[30] Available via anonymous ftp at ftp.aavso.org
[31] The VLA is operated by the National Radio Astronomy Observatory, a facility of the NSF operated under cooperative agreement by Associated Universities, Inc.

Table 1
Optical/NIR Observations of GRB 060418

UT Date[a]	Telescope/Instrument	Time Since Burst[b] (s)	Filter	Exposure Time (s)	Magnitude[c]
2006 Apr 18.2261	PAIRITEL	1.161×10^4	J	4206.5	17.11 ± 0.06
2006 Apr 18.2261	PAIRITEL	1.161×10^4	H	4206.5	16.17 ± 0.10
2006 Apr 18.2261	PAIRITEL	1.161×10^4	K_s	4206.5	15.43 ± 0.11
2006 Apr 18.2429	P60	1.011×10^4	R_C	600.0	18.60 ± 0.06
2006 Apr 18.2511	P60	1.083×10^4	i'	600.0	18.57 ± 0.07
2006 Apr 18.2593	P60	1.153×10^4	V_C	600.0	19.36 ± 0.09
2006 Apr 18.2675	P60	1.224×10^4	R_C	600.0	18.83 ± 0.06
2006 Apr 18.2757	P60	1.296×10^4	i'	600.0	18.80 ± 0.08
2006 Apr 18.2841	P60	1.368×10^4	V_C	600.0	19.50 ± 0.13
2006 Apr 18.2924	P60	1.440×10^4	R_C	600.0	19.03 ± 0.09
2006 Apr 18.3009	P60	1.513×10^4	i'	600.0	19.06 ± 0.09
2006 Apr 18.3021	PAIRITEL	1.545×10^4	J	682.8	17.57 ± 0.08
2006 Apr 18.3021	PAIRITEL	1.545×10^4	H	682.8	16.39 ± 0.09
2006 Apr 18.3021	PAIRITEL	1.545×10^4	K_s	682.8	16.19 ± 0.14
2006 Apr 18.3098	P60	1.590×10^4	V_C	600.0	19.61 ± 0.20
2006 Apr 18.3151	PAIRITEL	1.781×10^4	J	2283.8	17.55 ± 0.06
2006 Apr 18.3151	PAIRITEL	1.781×10^4	H	2283.8	16.70 ± 0.09
2006 Apr 18.3151	PAIRITEL	1.781×10^4	K_s	2283.8	16.32 ± 0.12
2006 Apr 18.3271	P60	1.740×10^4	R_C	600.0	19.38 ± 0.10
2006 Apr 18.3376	P60	1.830×10^4	i'	600.0	19.38 ± 0.09
2006 Apr 18.3465	P60	1.907×10^4	V_C	600.0	19.96 ± 0.15
2006 Apr 18.3553	P60	1.983×10^4	R_C	600.0	19.55 ± 0.11
2006 Apr 18.3567	PAIRITEL	2.140×10^4	J	2283.8	17.91 ± 0.08
2006 Apr 18.3567	PAIRITEL	2.140×10^4	H	2283.8	17.03 ± 0.09
2006 Apr 18.3567	PAIRITEL	2.140×10^4	K_s	2283.8	16.50 ± 0.20
2006 Apr 18.3642	P60	2.059×10^4	i'	600.0	19.52 ± 0.13
2006 Apr 18.3837	P60	2.258×10^4	V_C	1200.0	20.36 ± 0.15
2006 Apr 18.3917	P60	2.297×10^4	i'	600.0	19.61 ± 0.08
2006 Apr 18.3935	P60	2.343×10^4	R_C	1200.0	19.78 ± 0.09
2006 Apr 18.3983	PAIRITEL	2.501×10^4	J	2307.3	18.17 ± 0.08
2006 Apr 18.3983	PAIRITEL	2.501×10^4	H	2307.3	17.23 ± 0.12
2006 Apr 18.3983	PAIRITEL	2.501×10^4	K_s	2307.3	16.58 ± 0.15
2006 Apr 18.4222	P60	2.561×10^4	i'	600.0	19.90 ± 0.11
2006 Apr 18.4403	PAIRITEL	2.862×10^4	J	2283.8	18.38 ± 0.10
2006 Apr 18.4403	PAIRITEL	2.862×10^4	H	2283.8	17.57 ± 0.13
2006 Apr 18.4403	PAIRITEL	2.862×10^4	K_s	2283.8	16.39 ± 0.11
2006 Apr 18.4408	P60	2.722×10^4	R_C	600.0	20.31 ± 0.16
2006 Apr 18.4456	P60	2.793×10^4	V_C	1200.0	20.87 ± 0.23
2006 Apr 18.4544	P60	2.839×10^4	i'	600.0	19.96 ± 0.12
2006 Apr 18.4552	P60	2.877×10^4	R_C	1200.0	20.09 ± 0.12
2006 Apr 18.4818	PAIRITEL	3.174×10^4	J	1672.6	18.52 ± 0.11
2006 Apr 18.4818	PAIRITEL	3.174×10^4	H	1672.6	17.94 ± 0.18
2006 Apr 18.4818	PAIRITEL	3.174×10^4	K_s	1672.6	17.22 ± 0.18
2006 Apr 18.4864	P60	3.116×10^4	i'	600.0	20.02 ± 0.13
2006 Apr 19.3560	P60	1.072×10^5	R_C	1800.0	>21.02
2006 Apr 19.3581	PAIRITEL	1.079×10^5	J	2283.8	>19.06
2006 Apr 19.3581	PAIRITEL	1.079×10^5	H	2283.8	>18.61
2006 Apr 19.3581	PAIRITEL	1.079×10^5	K_s	2283.8	>17.89
2006 Apr 19.3669	P60	1.081×10^5	i'	1800.0	>21.49
2006 Apr 19.3782	P60	1.091×10^5	V_C	1800.0	>21.36
2006 Apr 20.3405	P60	1.920×10^5	R_C	1800.0	>21.75
2006 Apr 20.3535	P60	1.931×10^5	i'	1800.0	>22.19
2006 Apr 19.2870	P200/LFC	1.002×10^5	r'	300.0	22.07 ± 0.10
2006 Apr 19.2954	P200/LFC	1.009×10^5	i'	300.0	21.73 ± 0.10
2006 Apr 19.3033	P200/LFC	1.016×10^5	z'	300.0	21.52 ± 0.29
2006 Apr 19.3122	P200/LFC	1.024×10^5	g'	300.0	22.75 ± 0.15
2006 Apr 22.5584	Keck/LRIS	3.833×10^5	R_C	1200.0	23.31 ± 0.08
2006 Apr 22.5590	Keck/LRIS	3.835×10^5	g'	1500.0	>23.08
2006 May 9.4161	*HST*/ACS	1.839×10^6	*F625W*	4220.0	27.06 ± 0.15
2006 May 9.6130	*HST*/ACS	1.856×10^6	*F775W*	4220.0	26.96 ± 0.19
2006 May 20.2953	*HST*/ACS	2.779×10^6	*F625W*	5500.0	>27.53
2006 May 20.4926	*HST*/ACS	2.796×10^6	*F775W*	3700.0	>26.93
2006 Jun 1.7528	*HST*/ACS	3.855×10^6	*F625W*	8772.0	>28.04
2006 Jun 2.0193	*HST*/ACS	3.879×10^6	*F775W*	8772.0	>27.51
2006 Jul 11.1211	*HST*/ACS	7.343×10^6	*F625W*	8772.0	>28.16
2006 Jul 12.5207	*HST*/ACS	7.378×10^6	*F775W*	8772.0	>28.10
2006 Jul 13.1036	*HST*/ACS	7.428×10^6	*F555W*	4386.0	>27.53

Notes.
[a] UT at beginning of exposure.
[b] Time from midpoint of exposure to *Swift*/BAT trigger.
[c] Reported magnitudes have not been corrected for Galactic extinction ($E(B-V) = 0.22$ mag; Schlegel et al. 1998). Observations in the V_C, R_C, J, H, and K_s filters are referenced to Vega, while all other filters use the AB magnitude system (Oke & Gunn 1983).

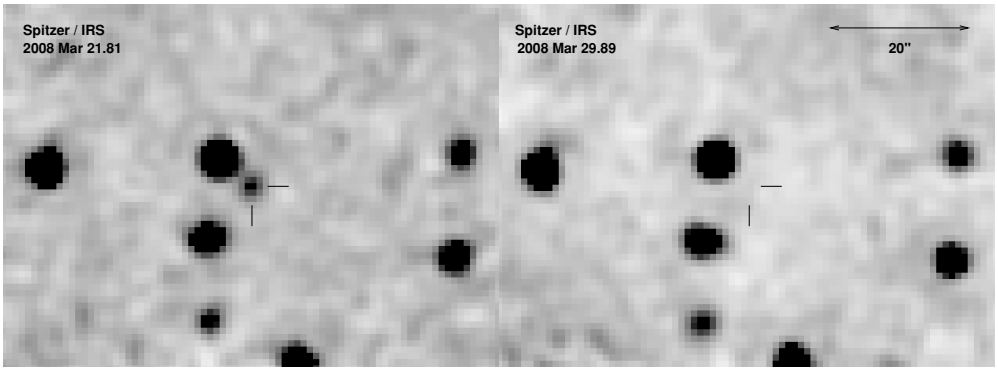

Figure 6. *Spitzer* imaging of GRB 080319B. We obtained target-of-opportunity observations of the afterglow of GRB 080319B in peak-up imaging mode (i.e., with the blue 15.8 μm filter) of the Infrared Spectrograph (IRS). Left: IRS peak-up images obtained beginning at 2008 March 21.81. The afterglow is indicated with the black tick marks. Right: IRS peak-up images of the identical field beginning at 2008 March 29.89. The afterglow has faded below the sensitivity limit at this time. Both images are oriented with north up and east to the left and have been smoothed with a two-pixel Gaussian filter.

Table 2
Radio Observations of GRB 060418

UT Date[a]	Time Since Burst[b] (d)	Frequency (GHz)	Flux Density (μJy)
2006 Apr 19.50	1.37	8.46	105 ± 45
2006 Apr 22.43	4.30	8.46	148 ± 44
2006 Apr 25.42	7.29	8.46	242 ± 59
2006 Apr 27.25	9.12	8.46	113 ± 43
2006 May 4.15	16.02	8.46	184 ± 39
2006 May 6.20	18.07	8.46	158 ± 31
2006 May 9.17	21.04	8.46	61 ± 42
2006 May 11.17	23.04	8.46	136 ± 36
2006 Jun 8.21	51.08	8.46	30 ± 39
2006 Jun 25.27	68.14	8.46	−3 ± 31

Notes.
[a] UT at midpoint of exposure.
[b] Time from midpoint of exposure to *Swift*/BAT trigger.

Table 3
Radio/Submillimeter Observations of GRB 080319B

UT Date[a]	Time Since Burst[b] (d)	Frequency (GHz)	Flux Density[c] (μJy)
2008 Mar 20.48	1.11	95.0	123 ± 250
2008 Mar 21.56	2.30	4.86	204 ± 40
2008 Mar 21.56	2.30	8.46	232 ± 42
2008 Mar 21.81	2.55	1.90×10^4	35.7 ± 3.9
2008 Mar 26.48	7.22	4.86	167 ± 61
2008 Mar 26.48	7.22	8.46	8 ± 55
2008 Mar 29.89	10.63	1.90×10^4	<8.0
2008 Dec 25.83	281.57	1.46	−9 ± 14

Notes.
[a] UT at midpoint of exposure.
[b] Time from midpoint of exposure to *Swift*/BAT trigger.
[c] Upper limits are reported as 2σ rms per beam area.

GRB 080319B was observed with the VLA at 4.8 and 8.5 GHz at two epochs in the first week after the burst (Soderberg et al. 2008). Both observations took place when the array was in the "C" configuration. We also observed the afterglow location for 33 hr between 2008 December 20 and 2009 January 4 at 1.46 GHz to search for late-time emission. The afterglow was not detected to a 2σ upper limit of <28 μJy.

The results of our millimeter and radio monitoring of GRB 080319B are shown in Figure 7 and Table 3, along with the previously published X-ray and optical light curves.

3. BROADBAND MODELING EFFORTS

In the standard "fireball" formulation (e.g., Piran 2005), afterglow emission is powered by synchrotron radiation from relativistic electrons in the circumburst medium accelerated by an outgoing blast wave. The resulting spectrum is well described as a series of broken power laws with three characteristic frequencies: ν_a, the frequency below which the radiation is self-absorbed; ν_m, the characteristic frequency of the emitting electrons; and ν_c, the frequency above which electrons are able to cool efficiently through radiation (Granot & Sari 2002).

The temporal evolution of the afterglow depends on the density profile of the circumburst medium. We consider here two possibilities: a constant-density circumburst medium [$\rho(r) \propto r^0$], as would be expected in an environment similar to the interstellar medium (ISM; Sari et al. 1998), and a wind-like environment [$\rho(r) \propto r^{-2}$], as would be the case for a massive-star progenitor shedding its outer envelope at a constant rate before core collapse (Chevalier & Li 2000).

GRBs are believed to be highly collimated explosions (Rhoads 1999; Sari et al. 1999). At early times, observers only notice emission from a narrow cone (opening angle $\theta \approx \Gamma^{-1}$, where Γ is the Lorentz factor of the expanding shock) due to relativistic beaming. The resulting evolution therefore mimics an isotropic explosion. As the shock slows, however, lateral spreading of the jet becomes important, and the observer eventually notices "missing" emission from wider angles. This hydrodynamic transition manifests itself as an achromatic steepening in the afterglow light curve. Measuring the time of this jet break (t_j) allows us to infer the opening angle of the outflow (θ).

Our objective here is to translate the observed three critical frequencies, together with the peak flux density ($F_{\nu,\max}$) and the jet-break time (t_j), into a physical description of the outflow. In particular, we shall attempt to estimate seven parameters: $E_{\rm KE}$, the kinetic energy of the blast wave; n, the density of the circumburst medium; ϵ_e, the fraction of the total energy apportioned to electrons; ϵ_B, the fraction of the total energy apportioned to the magnetic field; p, the electron power-law index; A_V, the host-galaxy extinction; and θ, the jet opening angle. We make use of the software described by Yost et al. (2003), a multi-parameter fitting program incorporating the standard afterglow formulation, as well as corrections for radiative losses and inverse-Compton emission (Sari & Esin 2001).

To account for differences in instrumental configurations, we have applied a 5% cross-calibration uncertainty to all data

Table 4
GRB 050820A Forward-shock Best-fit Parameters

Medium Type[a]	$E_{\rm KE,iso}$ (10^{52} erg)	n (cm^{-3})	ϵ_e (%)	ϵ_B (%)	θ ($^\circ$)	p	A_V(host) (mag)	$\chi^2_{\rm r}$ (dof)
ISM-1	537^{+80}_{-95}	$0.18^{+0.12}_{-0.07}$	13 ± 2	$0.0022^{+0.0011}_{-0.0004}$	$6.6^{+0.5}_{-0.3}$	1.75 ± 0.02	$0.11^{+0.03}_{-0.02}$	1.34 (76)
ISM-2	410^{+19}_{-25}	$(3.9 \pm 1.0) \times 10^{-4}$	14^{+2}_{-1}	$1.3^{+0.3}_{-0.1}$	3.0 ± 0.1	$2.30^{+0.03}_{-0.04}$	<0.049[b]	1.31 (76)

Notes.
[a] Radial profile of the circumburst medium. $\rho \propto r^0$ for an ISM-like medium; $\rho \propto r^{-2}$ for a wind-like medium.
[b] We are only able to calculate an upper limit for the host extinction in this case.

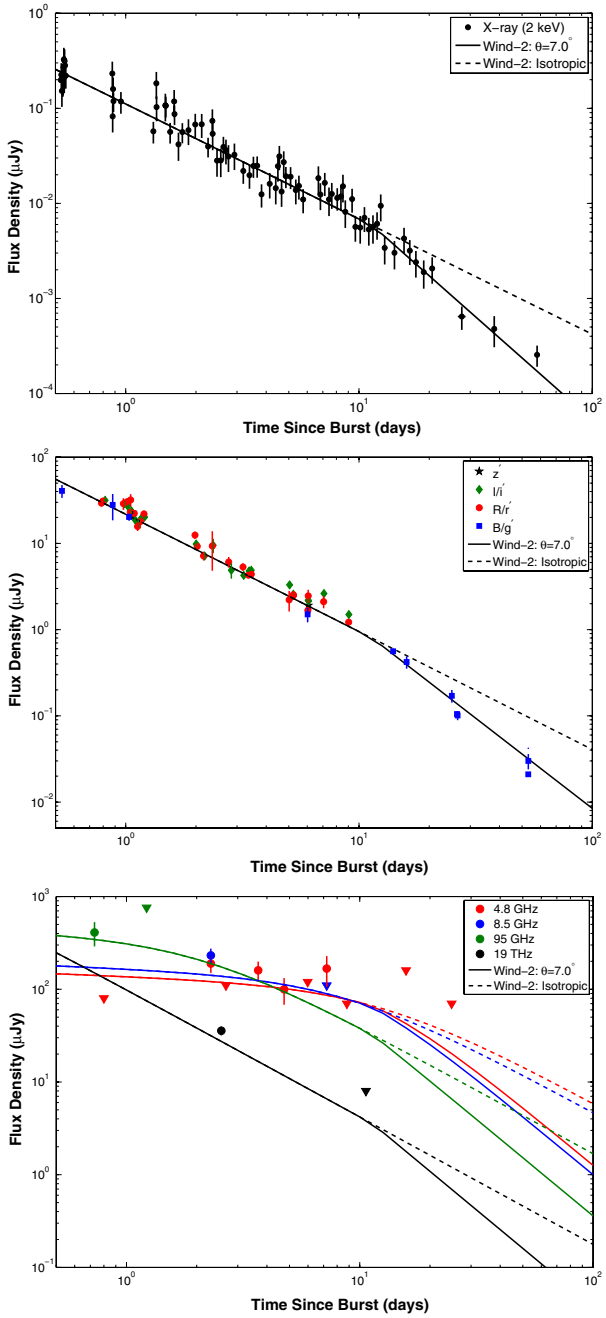

Figure 7. X-ray (top panel), optical (middle panel), and radio (bottom panel) light curves of GRB 080319B. The preferred model (Wind-2—Table 5) is plotted as a solid line, while the identical model for an isotropic explosion is shown as a dashed line. Both the X-ray and optical show a break at $t \approx 10$ days. The radio afterglow is too faint at this time to see evidence for collimation. We have left out the late-time ($t > 10$ days) r', i', and z' data from our fits due to the presence of contaminating SN emission.

(A color version of this figure is available in the online journal.)

points before calculating the models. All reported uncertainties have been determined using a Markov Chain Monte Carlo bootstrap analysis with 1000 trials and represent only statistical errors associated with the fit. Systematic errors associated with model uncertainties are likely to be much larger and difficult to estimate.

3.1. GRB 050820A

The optical and X-ray light curves of GRB 050820A exhibit a dramatic rebrightening at $t \approx 220$ s, both jumping in concert with a strong rise in the γ-ray emission (Vestrand et al. 2006; Cenko et al. 2006b). We therefore remove all X-ray and optical points at early times ($t < 0.1$ days) from our fitting routines. Likewise, the radio light curve exhibits a bright flare at $t \approx 1$ day that is probably due to reverse-shock emission (Cenko et al. 2006b). Since our modeling software only includes contributions from the forward shock, we include only radio observations at $t > 5$ days in our models.

The best-fit afterglow models for GRB 050820A are plotted in Figure 3, and the relevant physical parameters are provided in Table 4. As discussed by Cenko et al. (2006b), the optical light curve exhibits a distinct break between the last ground-based optical detection at $t \approx 7$ days and the *HST* observations at $t \approx 36$ days. The additional late-time X-ray data firmly establish the presence of this break in the X-ray bandpass as well, cementing the explanation as a jet break. The radio data at late times are not sufficient to distinguish between a beamed and isotropic outflow.

For a constant-density circumburst medium, we find two solutions with somewhat different model parameters but similar overall fit quality, and both are presented in Table 4. Though values of the electron index p less than 2 require a somewhat artificial cutoff to keep the total energy carried by the electrons finite, we slightly prefer the model with $p = 1.75$ (see, e.g., Bhattacharya 2001 for a discussion of afterglows with electron index $p < 2$). Several previous studies have suggested a relatively wide distribution of electron-index values (Shen et al. 2006; Starling et al. 2008; Curran et al. 2009). In this case, the density scale is more in line with our expectation that long-duration GRBs inhabit dense regions of recent star formation, as well as previous GRB afterglow modeling results (e.g., Panaitescu & Kumar 2002; Yost et al. 2003). Though the fraction of the total energy partitioned to the magnetic field (ϵ_B) is small, comparable values have been inferred for several other previous GRBs (e.g., Panaitescu & Kumar 2002).

Most importantly for our purposes, the kinetic energy of the afterglow ($E_{\rm KE}$) and the jet opening angle (θ) are relatively similar in the two models. Though both require extremely large isotropic kinetic energies, the values inferred here are only an order of magnitude larger than the prompt γ-ray energy release. This modest γ-ray conversion efficiency ($\eta_\gamma \equiv E_\gamma/[E_\gamma + E_{\rm KE}] \approx 10\%$) is consistent with theoretical predictions of

Table 5
GRB 060418 Forward-shock Best-fit Parameters

Medium Type[a]	$E_{\rm KE,iso}$ (10^{52} erg)	n/A_*[b] (cm^{-3}/g cm^{-1})	ϵ_e (%)	ϵ_B (%)	θ (°)	p	A_V(host) (mag)	$\chi^2_{\rm r}$ (dof)
ISM	$3.2^{+1.2}_{-0.6}$	$0.18^{+0.08}_{-0.06}$	33[c]	31^{+2}_{-1}	$13.9^{+2.1}_{-1.6}$	2.06 ± 0.01	0.08 ± 0.03	1.15 (82)
Wind	$0.12^{+0.03}_{-0.01}$	0.35 ± 0.12	6^{+1}_{-2}	15^{+14}_{-1}	$22.5^{+0.9}_{-2.5}$	$1.97^{+0.02}_{-0.04}$	$<10^{-4}$[d]	1.10 (81)

Notes.
[a] Radial profile of the circumburst medium. $\rho \propto r^0$ for an ISM-like medium; $\rho \propto r^{-2}$ for a wind-like medium.
[b] For a wind-like medium, the density parameter is better known as A_*, where $\rho \equiv 5 \times 10^{11} A_* r^{-2}$.
[c] The best fit was achieved with ϵ_e fixed to its equipartition value.
[d] We could only calculate an upper limit for the host extinction.

Table 6
GRB 080319B Forward-shock Best-fit Parameters

Medium Type[a]	$E_{\rm KE,iso}$ (10^{52} erg)	A_*[b] (cm^{-3}/g cm^{-1})	ϵ_e (%)	ϵ_B (%)	θ (°)	p	A_V(host) (mag)	$\chi^2_{\rm r}$ (dof)
Wind-1	$8.0^{+0.8}_{-0.5}$	$0.0056^{+0.0004}_{-0.0003}$	11 ± 1	33[c]	3.6 ± 0.2	2.10 ± 0.02	<0.04[d]	1.13 (157)
Wind-2	$4.9^{+3.2}_{-0.1}$	0.015 ± 0.005	$0.99^{+0.5}_{-0.01}$	33[c]	$7.0^{+0.7}_{-0.1}$	1.85 ± 0.02	$0.07^{+0.04}_{-0.02}$	1.12 (157)

Notes.
[a] Radial profile of the circumburst medium. $\rho \propto r^0$ for an ISM-like medium; $\rho \propto r^{-2}$ for a wind-like medium.
[b] For a wind-like medium, the density parameter is better known as A_*, where $\rho \equiv 5 \times 10^{11} A_* r^{-2}$.
[c] The best fit was achieved with ϵ_B fixed to its equipartition value.
[d] We could only calculate an upper limit for the host extinction.

the internal-shock model (Kobayashi et al. 1997; Daigne & Mochkovitch 1998).

The jet-break time occurs somewhat earlier than originally suggested by Cenko et al. (2006b). This is due to a combination of improved constraints from the X-ray afterglow coupled with a shallower post-break decay index inferred for the $p = 1.75$ model.

We were unable to obtain any high-quality fits to the afterglow of GRB 050820A assuming a wind-like circumburst medium. We shall return to the lack of evidence for massive-star progenitors from GRB afterglow modeling in Section 5.

3.2. GRB 060418

The most striking feature in the light curve of GRB 060418 is a bright X-ray flare at $t \approx 300$ s (Falcone et al. 2006b). Such flares have been reported in a large fraction of *Swift* XRT light curves (Falcone et al. 2007), and are widely believed to be caused by late-time energy injection from the central engine (Zhang et al. 2006). These X-ray flares can in some cases contribute a significant fraction of the prompt energy release to the total energy budget, and therefore have a large effect on the post-flare decay (Falcone et al. 2007). Rapid variability in the X-ray light curve of GRB 060418, inconsistent with standard afterglow models, is seen as late as several hours after the burst. Like GRB 050820A, we therefore only include observations at $t > 0.1$ days in our broadband modeling analysis.

The resulting fits and best-fit parameters are shown in Figure 4 and Table 5. Again, a clear break is seen in the optical light curve at late times ($t \approx 8$ days). The X-ray afterglow has dropped below the XRT threshold at this time. However, the radio afterglow is still detected and exhibits some evidence for a steepening decay consistent with that seen in the optical. Unfortunately, the break time is not very well constrained, either in the optical or radio bands. Though not entirely conclusive, we consider this relatively strong evidence in support of collimation.

Unlike most previously modeled afterglows, our results indicate that the electron cooling frequency (ν_c) fell below the optical bands over the duration of our observations. The forward-shock emission above ν_c is independent of the circumburst medium profile, leading to indistinguishable fits in the X-ray and optical bandpasses. While the radio behavior is divergent at early and late times, our observations are not sufficient to conclusively distinguish between the two models. Since the wind model provides a slightly better fit and does not require microphysical parameters held fixed at or near equipartition, we shall adopt it for the remainder of the work.

The primary drawback of the wind-like scenario, however, is the extremely high γ-ray efficiency. Somehow the physical process generating the prompt emission must have been capable of converting $\sim$99% of the outgoing blast-wave energy to γ-rays, while most internal-shock models predict a maximum γ-ray efficiency of $\sim$10% (Kobayashi et al. 1997; Daigne & Mochkovitch 1998). We shall return to this issue in Section 4.

3.3. GRB 080319B

Several groups (e.g., Racusin et al. 2008; Bloom et al. 2009; Woźniak et al. 2009; Pandey et al. 2009) have presented detailed observations of the early afterglow of GRB 080319B, revealing a complex behavior not easily understood in the context of the standard fireball model. In particular, we note that the optical spectral index ($\beta_{\rm O}$) evolves dramatically at early times, and as late as 0.5 days after the burst is too shallow to be accommodated by our forward-shock models ($\beta_O \lesssim 0.2$; Bloom et al. 2009). We therefore consider the evolution of the afterglow only at $t > 0.5$ days.

In addition, the late-time ($t \gtrsim 10$ days) optical light curve exhibits a pronounced red bump not seen in the X-rays that has been attributed to emission from an underlying SN (Tanvir et al. 2008; Bloom et al. 2009). Such features have now been seen in many relatively nearby GRB optical afterglows (Zeh et al. 2004), and are not accounted for in our synchrotron formulation. We therefore leave all r', i', and z' measurements out of our models at $t > 10$ days.

The resulting fits are plotted in Figure 7, with the model parameters presented in Table 6. As was pointed out by Racusin

et al. (2008) and most convincingly by Tanvir et al. (2008), both the X-ray and optical light curves exhibit a break at $t \approx 12$ days. The break is only clearly visible in the redder optical bands after including the contribution from the underlying SN. Here, the radio observations are unable to provide any constraints on the presence of a jet break, as the radio afterglow was comparably faint and only detected over the first week of observations.

We find that two models provide a reasonable fit to the broadband data, and both require a wind-like circumburst environment. The parameters derived for the first model, with $p = 2.10$, are broadly similar to those derived for the "wide" jet (see below) by Racusin et al. (2008), with one notable exception: ϵ_B differs by 2 orders of magnitude (fixed at equipartition in our model, compared with 3×10^{-3} in Racusin et al. 2008). Taken together, we find that the model parameters provided by Racusin et al. (2008) give a relatively poor fit to the late-time data, particularly in the optical bands. Unlike Pandey et al. (2009), we cannot find any reasonable broadband fits for ISM models; however, these authors are unable to reproduce the observed X-ray behavior regardless of the circumburst environment.

An alternate model, with $p = 1.85$, provides a marginally better fit to the data. Since the inferred density is slightly larger and more in line with that of previous GRB afterglows, we adopt this as our preferred model for the afterglow of GRB 080319B. We note again that the discrepancy between the two competing models is relatively small with respect to the afterglow energy and opening angle.

Racusin et al. (2008) have incorporated the early-time data into their model of GRB 080319B by invoking a double-jetted system: the high-energy emission is focused in a narrow ($\theta \approx 0.^\circ 2$) jet that dominates the early afterglow ($t \lesssim 0.5$ days), while the material at lower Lorentz factor powering the late-time afterglow is channeled into a wider jet ($\theta \approx 4^\circ$). Such a configuration is not without precedent and has been invoked to explain multiple breaks in the light curve of GRB 030329 (e.g., Berger et al. 2003b; van der Horst et al. 2005). Explaining the early-time emission from GRB 080319B is beyond the scope of this work; however, we consider the implications of multiple-jet models in Section 5.

3.4. GRBs 050904 and 070125

Finally, for completeness we include here a brief summary of the primary results from the modeling of GRB 050904 (Frail et al. 2006) and GRB 070125 (Chandra et al. 2008).

To date, GRB 050904 is the third most distant spectroscopically confirmed GRB ($z = 6.295$; Kawai et al. 2006; Haislip et al. 2006). The optical and X-ray light curves exhibit a prominent break at $t = 2.6 \pm 1.0$ days (Tagliaferri et al. 2005), resulting in an opening angle of $\theta \approx 8^\circ$. The afterglow was notable for an extremely large inferred density: $n \approx 700$ cm^{-3} for an isotropic circumburst medium. Even after applying a collimation correction, the total energy release from GRB 050904 was in excess of 10^{52} erg, making it one of the most energetic explosions ever detected.

Although *Swift* did not trigger immediately on GRB 070125, the γ-ray emission was bright enough to be detected by both Konus/*Wind* and *RHESSI*, providing superb coverage of the high-energy properties of this event (Bellm et al. 2008). The radio afterglow of GRB 070125 was one of the brightest in the *Swift* era, making it an ideal source for broadband modeling. A clear break is seen in the optical light curve at $t \approx 4$ days (Mirabal et al. 2007). While the X-ray light curve also undergoes a steepening around this time, it occurs slightly later than in the optical bandpass. This may be due to the effects of inverse-Compton emission dominating the X-ray afterglow at this time. The circumburst density inferred for GRB 070125 was also relatively high ($n \approx 40$ cm^{-3}), resulting in a strongly self-absorbed radio spectrum.

The relevant energy properties of all five of the events in our sample are summarized in Table 7.

Table 7
Collimation and Energetics of *Swift* GRBs

GRB	$t_{\rm jet}$ (d)	θ ($^\circ$)	E_γ (10^{51} erg)	$E_{\rm KE}$ (10^{51} erg)
050820A	$11.1^{+0.1}_{-1.7}$	$6.6^{+0.5}_{-0.3}$	$6.4^{+3.2}_{-1.5}$	$35.6^{+11.3}_{-9.4}$
050904	2.6 ± 1.0	8.0	$12.9^{+6.6}_{-3.9}$	$8.6^{+8.4}_{-4.3}$
060418	$7.6^{+2.0}_{-2.2}$	$22.5^{+0.9}_{-2.5}$	$3.0^{+3.8}_{-1.1}$	$0.94^{+0.22}_{-0.35}$
070125	$3.69^{+0.03}_{-0.07}$	13.2 ± 0.6	$25.3^{+5.1}_{-4.6}$	$1.7^{+0.4}_{-0.2}$
080319B	$11.8^{+0.8}_{-1.3}$	$7.0^{+0.7}_{-0.1}$	$10.2^{+3.2}_{-0.1}$	$0.35^{+0.38}_{-0.01}$

4. DISCUSSION

In the previous section, we provided model fits to the broadband afterglows of five *Swift* GRBs, all of which exhibit evidence for a collimated, relativistic outflow. In some cases, the breaks are clearly visible across the X-ray, optical, and radio bandpasses (e.g., GRB 070125), while in others the data are insufficient to verify the achromatic nature of the observed break (e.g., the X-rays for GRB 060418). Regardless, the fact that all five events are consistent with a beamed outflow is in marked contrast to previous searches for jet-break candidates in *Swift* events (Panaitescu 2007; Kocevski & Butler 2008; Racusin et al. 2009; Liang et al. 2008).

The most natural explanation for this discrepancy is the role of selection effects. As is evident from Figure 1, the heightened sensitivity of *Swift* is preferentially selecting GRBs with smaller $E_{\gamma,\rm iso}$ values compared with pre-*Swift* missions. The bandpass likely exacerbates this effect: the observed correlation between the peak energy of the prompt γ-ray spectrum ($E_{\rm p}$) and $E_{\gamma,\rm iso}$ (Amati 2006) further suggests that *Swift* is detecting an underluminous sample with respect to previous missions having extended high-energy coverage.

The result is that *Swift* jet breaks should occur on average later than those of pre-*Swift* events, making them more difficult to observe (for a given sensitivity limit). Such an effect was predicted (in the context of the structured jet model) by Perna et al. (2003). GRB 060418 offers an illustrative example; with $E_{\gamma,\rm iso} = 10^{53}$ erg, it falls in the 80th percentile of the *Swift* $E_{\gamma,\rm iso}$ distribution, and with $t_{\rm j} = 7.6$ days, the break occurred at $R \approx 24.5$ mag. The X-rays were already too faint at this time to be detected, and the only reason for the optical detection was the deep *HST* imaging. Given the typical follow-up capabilities of a medium-aperture telescope, jet breaks are virtually undetectable for a majority of *Swift* GRBs (Dai et al. 2008; Kocevski & Butler 2008). In fact, some of the faintest events (in terms of $E_{\gamma,\rm iso}$) may be isotropic and still consistent with our observed energetics distribution.

In Figure 8, we plot the observed jet-break times for our sample as a function of $E_{\gamma,\rm iso}$ compared to the pre-*Swift* sample from Friedman & Bloom (2005). The solid line indicates a constant collimation-corrected prompt energy release of $E_\gamma \approx 10^{51}$ erg. We wish to emphasize that the derived collimation angle is only weakly dependent on two model parameters: n and η_γ (both to the 1/8 power). Consequently, though the afterglow

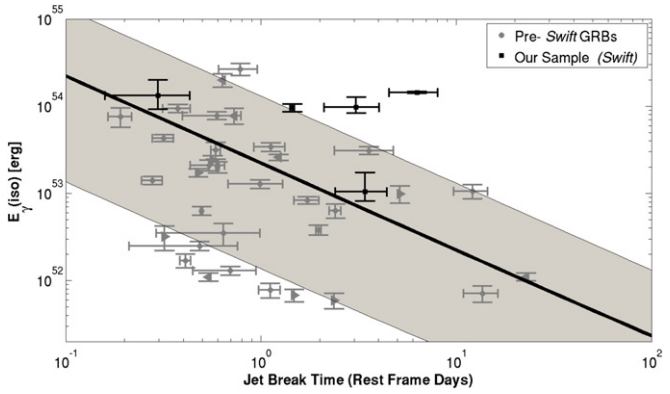

Figure 8. Afterglow jet-break time (rest frame) as a function of $E_{\gamma,\rm iso}$. The thick solid line represents a constant collimation-corrected prompt energy release of $E_\gamma \approx 10^{51}$ erg assuming a constant-density circumburst medium with density $n = 0.1\,{\rm cm}^{-3}$ and a γ-ray efficiency $\eta_\gamma = 20\,\%$. The actual relation between the jet-break time and the opening angle depends weakly on these two parameters: the shaded region indicates the effect of varying these values over nearly the entire range observed in long-duration GRB afterglows ($n = 0.01$–$100\,{\rm cm}^{-3}$, $\eta_\gamma = 1\%$–$90\,\%$). The events in our sample have on average larger jet-break times than analogous pre-*Swift* events. This result suggests that the E_γ distribution is wider than previously thought in a relatively model-independent manner. Pre-*Swift* events have been compiled from Friedman & Bloom (2005).

(A color version of this figure is available in the online journal.)

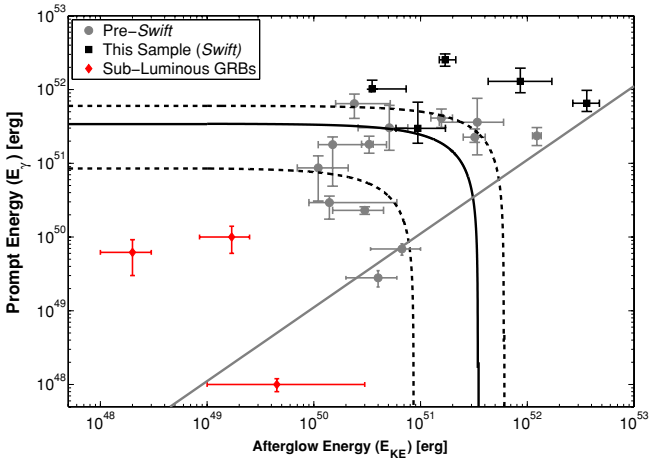

Figure 9. Two-dimensional ($E_{\rm KE} + E_{\gamma,\rm iso}$) relativistic energy release from long-duration GRBs. Neglecting the most nearby, underluminous GRBs (GRBs 980425, 031203, and 060218), pre-*Swift* events are clustered around a total energy release of $\sim 3 \times 10^{51}$ erg (solid line; dashed lines show the rms of the distribution). With the exception of GRB 060418, all of the events in our sample fall outside this distribution, typically with $E_{\rm total} \gtrsim 10^{52}$ erg. The solid gray line reflects a constant γ-ray efficiency of $\eta_\gamma = 0.1$. That so many of the observed events fall above this line suggests that internal shocks may not be responsible for the generation of the prompt γ-ray emission. References—Panaitescu & Kumar (2002): GRBs 990123, 990510, 991208, 991216, 000301C, 010222; Yost et al. (2003): GRBs 970508, 980703, 000926; Berger et al. (2004): GRBs 970508, 980703; Chevalier et al. (2004): GRB 020405; Berger et al. (2001): GRB 000418; Berger et al. (2003b): GRB 030329; Soderberg et al. (2004): GRB 020903; Li & Chevalier (1999): GRB 980425; Soderberg et al. (2004): GRB 031203; Soderberg et al. (2006): GRB 060218.

(A color version of this figure is available in the online journal.)

energy may be relatively uncertain, it is clear that the E_γ values derived for the events in our sample will be significantly larger than those of the typical pre-*Swift* GRB.

The final, collimation-corrected energy release from the events in our sample, both from the prompt γ-ray emission and powering the afterglow, is plotted in Figure 9. Also plotted are analogous results from previous studies of pre-*Swift* afterglows with broadband (X-ray, optical, *and* radio) coverage (see figure caption for references). With the exception of the most nearby events (diamonds), the total relativistic (neglecting, for example, SN emission) energy release ($E_\gamma + E_{\rm KE}$) from pre-*Swift* GRBs was relatively tightly clustered around a value of $\sim 3 \times 10^{51}$ erg (solid line in Figure 9). Clearly, the GRBs presented here are inconsistent with this distribution, preferentially falling at the high-energy end. Several events exceed 10^{52} erg in total energy release, something only achieved for a single event in the pre-*Swift* era (GRB 970508; Yost et al. 2003; Berger et al. 2004). Much as has been seen at the low-energy end, our results suggest that the true energy release from GRBs is relatively broad and capable of extending out to at least 10^{52} erg.

Finally, we return to the issue of γ-ray efficiency. As has also been seen in the pre-*Swift* era, the inferred γ-ray efficiency can often be dramatically higher than would be predicted from the internal-shock model ($\eta_\gamma \lesssim 0.10$; Kobayashi et al. 1997; Daigne & Mochkovitch 1998). The problem may be eased to some extent by the nature of our model parameters, as $E_{\rm KE}$ is measured at the time of the transition from fast to slow cooling, after which the shock may have lost a significant fraction of its initial energy (Chandra et al. 2008). However, this would necessarily increase the total energy budget, possibly at times to values approaching 10^{53} erg. An alternative possibility is that the γ-rays are produced via relativistic turbulence (Lazar et al. 2009; Narayan & Kumar 2009), where the γ-ray efficiency can approach unity. Such a model has been already been invoked for GRB 080319B (Kumar & Narayan 2009), and clearly merits further study.

Alternatively, if the flux distribution were dominated by small-scale fluctuations (of angular scale Γ^{-1}), this may cause a large variation in the energy distribution (the "patchy shell" model; Kumar & Piran 2000). This would have a particularly strong influence on E_γ, as the energy would be averaged over a much smaller physical scale, and could lead to large fluctuations in the value of η_γ.

5. CONCLUSIONS

In this work, we have presented model fits to the broadband afterglows of the *Swift* GRBs 050820A, 060418, and 080319B. Together with previous results from GRB 050904 and GRB 070125, we demonstrate all five events are consistent with our understanding of relativistic, collimated explosions. However, the inferred opening angles for several events are larger than would be expected if GRBs were truly standard candles. The result is a broad collimation-corrected energy distribution, with some events emitting in excess of 10^{52} erg.

It is at first glance somewhat surprising that *Swift* has discovered a large fraction of the most energetic GRBs. This may be due in large part to sample size. As can be seen from Figure 1, nearly all of the GRBs in our sample (except GRB 060418) were brighter (in terms of $E_{\gamma,\rm iso}$) than almost all of the pre-*Swift* GRBs having known redshifts. Even though the median $E_{\gamma,\rm iso}$ value of *Swift* bursts is smaller than in the pre-*Swift* sample, the increase in the total number of GRBs detected by *Swift* has enabled it to target the extreme ends of the energy distribution. These events must be relatively rare, or they would have been easily detected by previous high-energy missions.

Despite their rarity, the most energetic events provide some of the strongest constraints on possible progenitor models. The maximum energy release in magnetar models (Usov 1992) is $\sim 3 \times 10^{52}$ erg, which is set by the rotational energy of a

maximally rotating neutron star (see, e.g., Thompson et al. 2004; Metzger et al. 2007). The fact that several events in our sample approach this limit suggests that the central-engine remnant should be a black hole (at least for these hyper-energetic GRBs). With a lower bound on the collimation-corrected prompt energy release from GRB 080721 of $E_\gamma \gtrsim 10^{52}$ erg, Starling et al. (2009) reach a similar conclusion regarding the origin of this event.

A lingering question, then, is how to produce the long-lived ($t \gg \Delta t_{\rm GRB}$) central-engine activity seen commonly in *Swift* X-ray afterglows (e.g., Zhang et al. 2006), either from a neutron star or a black hole system. In the case of a rapidly spinning proto-neutron star, late-time energy injection through electromagnetic dipole radiation has long been suggested as a possible source of achromatic afterglow bumps (Dai & Lu 1998; Zhang & Mészáros 2001; Troja et al. 2007; Lyons et al. 2010). Alternatively, for black hole systems, changes in the structure of the accretion-disk system could drive an unsteady outflow at late times (Lazzati et al. 2008). Clearly, this issues merits further study in the future.

While our modeling generally provides reasonable physical parameters, the requirement in certain instances of a constant-density circumburst medium suggests caution against overinterpreting such results. In the case of radio SNe, where the shock expansion is Newtonian, the circumburst medium is consistently well fit with an r^{-2} density profile (Weiler & Sramek 1988). Despite the preponderance of evidence for the association of GRBs with massive stars (Woosley & Bloom 2006, and references therein), the evidence for a wind-blown medium is not secure for individual events (e.g., Chevalier et al. 2004; Panaitescu & Kumar 2000).

One possible explanation may be our relatively poor understanding of the final stages of stellar evolution. A variety of recent results, ranging from the discovery of fast-moving ($v \approx 6000$ km s^{-1}) material ejected from η Car (Smith 2008), to the dense circumstellar material partially powering the luminous ($M_V \approx -22$ mag) SN 2006gy (Ofek et al. 2007; Smith et al. 2007), to detection of a pre-SN outburst from SN 2006jc (Pastorello et al. 2007; Foley et al. 2007) and SN 2005gl (Gal-Yam & Leonard 2009), suggest that massive stars undergo violent periods of episodic mass loss in the late stages of stellar evolution. Future theoretical progress to pin down the expected density profile surrounding massive stars in the latest stages of stellar evolution at distances relevant to GRB afterglows ($\sim$1 pc) (e.g., Ramirez-Ruiz et al. 2005; Dwarkadas 2007), or alternatively, to more reliably infer the density profile from afterglow observations (e.g., van Eerten & Wijers 2009), might help to resolve this discrepancy

An additional concern, motivated by the double-jet models for GRB 030329 (Berger et al. 2003b; van der Horst et al. 2005) and GRB 080319B (Racusin et al. 2008), is our assumption that the entire relativistic outflow is collimated into a uniform jet with a single opening angle (the so-called top-hat model). A variety of other models for structured jets have been proposed, typically with the Lorentz factor of the outflow varying as a function of angle from the jet axis (see, e.g., Granot 2007 for a review). Though the double-jet model is no doubt a bit contrived, theoretical simulations of relativistic jets suggest that the top-hat model is overly simplistic (e.g., Zhang et al. 2004; Tchekhovskoy et al. 2008). It would also ease the sometimes extreme efficiency requirements if the γ-ray emission were more narrowly beamed than the afterglow. However, such models imply the existence of the so-called on-axis orphan afterglows, where the line of sight misses the γ-ray emission but an observer still sees a regular (on-axis) afterglow. The lack of such events to date limits the X-ray to γ-ray beaming factor ratio to $<$2:1, while future wide-field, high-cadence surveys will soon do the same for the optical (Nakar & Piran 2003).

Finally, we consider the future prospects for the study of the most energetic GRBs. As we suggested previously (Chandra et al. 2008), the recent launch of the *Fermi* satellite offers an incredible opportunity in this respect. The high-energy bandpass of the Large Area Telescope (LAT), extending out to hundreds of GeV, is ideally suited to target the bright end of the $E_{\gamma,\rm iso}$ distribution. Already in less than a year of operation, *Fermi* has detected two of the brightest GRBs ever, GRB 080916C (Abdo et al. 2009b; Greiner et al. 2009) and GRB 090323 (Ohno et al. 2009; Golenetskii et al. 2009b), with $E_{\gamma,\rm iso}$ in excess of 5×10^{54} erg. Coupled with the large Lorentz factor required to produce GeV photons, multi-wavelength campaigns targeted at such events are well positioned to search for early jet breaks when the afterglow is still bright. Together, synergistic *Swift* and *Fermi* observations in the coming years should be able to shed a good deal of light on the high end of the GRB energy distribution.

S.B.C. and A.V.F. acknowledge generous support from Gary and Cynthia Bengier, the Richard and Rhoda Goldman Fund, NASA/*Swift* grants NNG06GI86G and NNX09AL08G, and NSF grants AST–0607485 and AST–0908886. A.G. acknowledges support by the Israeli Science Foundation, an EU Seventh Framework Programme Marie Curie IRG fellowship and the Benoziyo Center for Astrophysics, a research grant from the Peter and Patricia Gruber Awards, and the William Z. and Eda Bess Novick New Scientists Fund at the Weizmann Institute. J.N.N. is supported by NASA contract NAS5-00136. T.P. acknowledges support from an ERC advanced research grant. P60 operations are funded in part by NASA through the *Swift* Guest Investigator Program (grant number NNG06GH61G). Based on observations made with the NASA/ESA *Hubble Space Telescope*, obtained from the Data Archive at the Space Telescope Science Institute, which is operated by the Association of Universities for Research in Astronomy, Inc., under NASA contract NAS 5-26555. These data are associated with program GO-10551. This work is based in part on observations made with the *Spitzer Space Telescope*, which is operated by the Jet Propulsion Laboratory, California Institute of Technology, under a contract with NASA. We thank the SSC Director for an award of discretionary time and the *Spitzer* Operations team for their quick response to our request. This publication has made use of data obtained from the *Swift* interface of the High-Energy Astrophysics Archive (HEASARC), provided by NASA's Goddard Space Flight Center. Support for CARMA construction was derived from the Gordon and Betty Moore Foundation, the Kenneth T. and Eileen L. Norris Foundation, the Associates of the California Institute of Technology, the states of California, Illinois, and Maryland, and the NSF. Ongoing CARMA development and operations are supported by the NSF under a cooperative agreement, and by the CARMA partner universities. PAIRITEL is operated by the Smithsonian Astrophysical Observatory (SAO) and was made possible by a grant from the Harvard University Milton Fund, a camera loan from the University of Virginia, and continued support of the SAO and UC Berkeley. The PAIRITEL project is further supported by NASA/*Swift* Guest Investigator grants NNG06GH50G and

NNX08AN84G. Some of the data presented herein were obtained at the W. M. Keck Observatory, which is operated as a scientific partnership among the California Institute of Technology, the University of California and the NASA; the observatory was made possible by the generous financial support of the W. M. Keck Foundation. The authors recognize and acknowledge the very significant cultural role and reverence that the summit of Mauna Kea has always had within the indigenous Hawaiian community; we are most fortunate to have the opportunity to conduct observations from this mountain.

Facilities: VLA, HST (ACS), *Swift* (XRT), Keck:I (LRIS), PO:1.5m, Hale (LFC), FLWO:2MASS (PAIRITEL), *Spitzer* (IRS), CARMA

REFERENCES

Abdo, A. A., et al. 2009a, ApJ, 706, L138
Abdo, A. A., et al. 2009b, Science, 323, 1688
Amati, L. 2006, MNRAS, 372, 233
Barthelmy, S. D., et al. 2005, Space Sci. Rev., 120, 143
Bellm, E. C., et al. 2008, ApJ, 688, 491
Berger, E., Kulkarni, S. R., & Frail, D. A. 2003a, ApJ, 590, 379
Berger, E., Kulkarni, S. R., & Frail, D. A. 2004, ApJ, 612, 966
Berger, E., et al. 2001, ApJ, 556, 556
Berger, E., et al. 2003b, Nature, 426, 154
Bhattacharya, D. 2001, Bull. Astron. Soc. India, 29, 107
Bloom, J. S., Frail, D. A., & Kulkarni, S. R. 2003, ApJ, 594, 674
Bloom, J. S., Starr, D. L., Blake, C. H., Skrutskie, M. F., & Falco, E. E. 2006, in ASP Conf. Ser. 351, Astronomical Data Analysis Software and Systems XV, ed. C. Gabriel et al. (San Francisco, CA: ASP), 751
Bloom, J. S., et al. 2009, ApJ, 691, 723
Bock, D. C.-J., Chandra, P. C., Kulkarni, S. R., Frail, D. A., & Cenko, S. B. 2008, GRB Coordinates Network, 7493, 1
Burrows, D. N., et al. 2005a, Space Sci. Rev., 120, 165
Burrows, D. N., et al. 2005b, Science, 309, 1833
Butler, N. R., & Kocevski, D. 2007, ApJ, 663, 407
Butler, N. R., Kocevski, D., Bloom, J. S., & Curtis, J. L. 2007, ApJ, 671, 656
Cenko, S. B., et al. 2006a, PASP, 118, 1396
Cenko, S. B., et al. 2006b, ApJ, 652, 490
Cenko, S. B., et al. 2009, ApJ, 693, 1484
Chandra, P., et al. 2008, ApJ, 683, 924
Chen, H.-W., et al. 2009, ApJ, 691, 152
Chevalier, R. A., & Li, Z.-Y. 2000, ApJ, 536, 195
Chevalier, R. A., Li, Z.-Y., & Fransson, C. 2004, ApJ, 606, 369
Cobb, B. E., Bailyn, C. D., van Dokkum, P. G., & Natarajan, P. 2006, ApJ, 645, L113
Cummings, J., et al. 2006, GRB Coordinates Network, 4975, 1
Curran, P. A., Starling, R. L. C., van der Horst, A. J., & Wijers, R. A. M. J. 2009, MNRAS, 395, 580
Curran, P. A., et al. 2007, MNRAS, 381, L65
Dai, Z. G., Liang, E. W., & Xu, D. 2004, ApJ, 612, L101
Dai, Z. G., & Lu, T. 1998, A&A, 333, L87
Dai, X., et al. 2008, ApJ, 682, L77
Daigne, F., & Mochkovitch, R. 1998, MNRAS, 296, 275
D'Elia, V., et al. 2009, ApJ, 694, 332
Donaghy, T. Q., et al. 2006, arXiv:astro-ph/0605570
Dwarkadas, V. V. 2007, ApJ, 667, 226
Falcone, A. D., Barthelmy, S. D., Burrows, D. N., Cummings, J. R., Gehrels, N., Hunsberger, S. D., Kennea, J. A., & Palmer, D. M. 2006a, GRB Coordinates Network, 4966, 1
Falcone, A. D., Burrows, D. N., & Kennea, J. 2006b, GRB Coordinates Network, 4973, 1
Falcone, A. D., et al. 2007, ApJ, 671, 1921
Fan, Y., & Piran, T. 2006, MNRAS, 369, 197
Filippenko, A. V. 2005, in White Dwarfs: Cosmological and Galactic Probes, ed. E. M. Sion, S. Vennes, & H. L. Shipman (Dordrecht: Springer), 97
Firmani, C., Avila-Reese, V., Ghisellini, G., & Ghirlanda, G. 2006, MNRAS, 372, L28
Foley, R. J., Smith, N., Ganeshalingam, M., Li, W., Chornock, R., & Filippenko, A. V. 2007, ApJ, 657, L105
Frail, D. A., Soderberg, A. M., Kulkarni, S. R., Berger, E., Yost, S., Fox, D. W., & Harrison, F. A. 2005, ApJ, 619, 994
Frail, D. A., et al. 2001, ApJ, 562, L55
Frail, D. A., et al. 2006, ApJ, 646, L99
Friedman, A. S., & Bloom, J. S. 2005, ApJ, 627, 1
Fruchter, A. S., & Hook, R. N. 2002, PASP, 114, 144
Gal-Yam, A., & Leonard, D. C. 2009, Nature, 458, 865
Gehrels, N., et al. 2004, ApJ, 611, 1005
Golenetskii, S., Aptekar, R., Mazets, E., Pal'Shin, V., Frederiks, D., Ulanov, M., & Cline, T. 2006, GRB Coordinates Network, 4989, 1
Golenetskii, S., et al. 2009a, GRB Coordinates Network, 9959
Golenetskii, S., et al. 2009b, GRB Coordinates Network, 9030, 1
Granot, J. 2007, RevMexAA Conf. Ser., 27, 140
Granot, J., & Sari, R. 2002, ApJ, 568, 820
Greiner, J., et al. 2009, A&A, 498, 89
Guetta, D., & Valle, M. D. 2007, ApJ, 657, L73
Haislip, J. B., et al. 2006, Nature, 440, 181
Kawai, N., et al. 2006, Nature, 440, 184
Kobayashi, S., Piran, T., & Sari, R. 1997, ApJ, 490, 92
Kocevski, D., & Butler, N. 2008, ApJ, 680, 531
Kumar, P., & Narayan, R. 2009, MNRAS, 395, 472
Kumar, P., & Panaitescu, A. 2008, MNRAS, 391, L19
Kumar, P., & Piran, T. 2000, ApJ, 535, 152
Lazar, A., Nakar, E., & Piran, T. 2009, ApJ, 695, L10
Lazzati, D., Perna, R., & Begelman, M. C. 2008, MNRAS, 388, L15
Li, Z.-Y., & Chevalier, R. A. 1999, ApJ, 526, 716
Liang, E.-W., Racusin, J. L., Zhang, B., Zhang, B.-B., & Burrows, D. N. 2008, ApJ, 675, 528
Lyons, N., O'Brien, P. T., Zhang, B., Willingale, R., Troja, E., & Starling, R. L. C. 2010, MNRAS, 402, 705
Metzger, B. D., Thompson, T. A., & Quataert, E. 2007, ApJ, 659, 561
Mirabal, N., Halpern, J., & Thorstensen, J. R. 2007, GRB Coordinates Network, 6096, 1
Nakar, E., & Piran, T. 2003, New Astron., 8, 141
Narayan, R., & Kumar, P. 2009, MNRAS, 394, L117
Nousek, J. A., et al. 2006, ApJ, 642, 389
Ofek, E. O., et al. 2007, ApJ, 659, L13
Ohno, M., Cutini, S., McEnery, J., Chiang, J., & Koerding, E. 2009, GRB Coordinates Network, 9021, 1
Oke, J. B., & Gunn, J. E. 1983, ApJ, 266, 713
Oke, J. B., et al. 1995, PASP, 107, 375
Panaitescu, A. 2007, MNRAS, 380, 374
Panaitescu, A., & Kumar, P. 2000, ApJ, 543, 66
Panaitescu, A., & Kumar, P. 2002, ApJ, 571, 779
Pandey, S. B., et al. 2009, A&A, 504, 45
Pastorello, A., et al. 2007, Nature, 447, 829
Perlmutter, S., et al. 1999, ApJ, 517, 565
Perna, R., Sari, R., & Frail, D. 2003, ApJ, 594, 379
Piran, T. 2005, Rev. Mod. Phys., 76, 1143
Pollack, L. K., Chen, H.-W., Prochaska, J. X., & Bloom, J. S. 2009, ApJ, 701, 1605
Prochaska, J. X., et al. 2007, ApJS, 168, 231
Racusin, J. L., et al. 2008, Nature, 455, 183
Racusin, J. L., et al. 2009, ApJ, 698, 43
Ramirez-Ruiz, E., García-Segura, G., Salmonson, J. D., & Pérez-Rendón, B. 2005, ApJ, 631, 435
Rau, A. 2009, GRB Coordinates Network, 9983
Rau, A., Connaughton, V., & Briggs, M. 2009, GRB Coordinates Network, 9057
Rhoads, J. E. 1999, ApJ, 525, 737
Riess, A. G., et al. 1998, AJ, 116, 1009
Sari, R., & Esin, A. A. 2001, ApJ, 548, 787
Sari, R., Piran, T., & Halpern, J. P. 1999, ApJ, 519, L17
Sari, R., Piran, T., & Narayan, R. 1998, ApJ, 497, L17
Schady, P., et al. 2007, MNRAS, 380, 1041
Schaefer, B. E. 2007, ApJ, 660, 16
Schlegel, D. J., Finkbeiner, D. P., & Davis, M. 1998, ApJ, 500, 525
Shen, R., Kumar, P., & Robinson, E. L. 2006, MNRAS, 371, 1441
Sirianni, M., et al. 2005, PASP, 117, 1049
Skrutskie, M. F., et al. 2006, AJ, 131, 1163
Smith, N. 2008, Nature, 455, 201
Smith, N., et al. 2007, ApJ, 666, 1116
Soderberg, A., Chandra, P., & Frail, D. 2008, GRB Coordinates Network, 7506
Soderberg, A. M., et al. 2004, Nature, 430, 648
Soderberg, A. M., et al. 2006, Nature, 442, 1014
Spergel, D. N., et al. 2007, ApJS, 170, 377
Starling, R. L. C., van der Horst, A. J., Rol, E., Wijers, R. A. M. J., Kouveliotou, C., Wiersema, K., Curran, P. A., & Weltevrede, P. 2008, ApJ, 672, 433
Starling, R. L. C., et al. 2009, MNRAS, 400, 90
Tagliaferri, G., et al. 2005, A&A, 443, L1
Tanvir, N. R., et al. 2008, arXiv:0812.1217
Tchekhovskoy, A., McKinney, J. C., & Narayan, R. 2008, MNRAS, 388, 551

Teplitz, H., Werner, M., Cenko, S. B., Kulkarni, S. R., & Rau, A. 2008, GRB Coordinates Network, 7509
Thompson, T. A., Chang, P., & Quataert, E. 2004, ApJ, 611, 380
Troja, E., et al. 2007, ApJ, 665, 599
Usov, V. V. 1992, Nature, 357, 472
van der Horst, A. J., Rol, E., Wijers, R. A. M. J., Strom, R., Kaper, L., & Kouveliotou, C. 2005, ApJ, 634, 1166
van der Horst, A. J., et al. 2008, A&A, 480, 35
van Eerten, H. J., & Wijers, R. A. M. J. 2009, MNRAS, 394, 2164
Vestrand, W. T., et al. 2006, Nature, 442, 172
Weiler, K. W., & Sramek, R. A. 1988, ARA&A, 26, 295
Woosley, S. E. 1993, ApJ, 405, 273
Woosley, S. E., & Bloom, J. S. 2006, ARA&A, 44, 507
Woźniak, P. R., Vestrand, W. T., Panaitescu, A. D., Wren, J. A., Davis, H. R., & White, R. R. 2009, ApJ, 691, 495
Yost, S. A., Harrison, F. A., Sari, R., & Frail, D. A. 2003, ApJ, 597, 459
Zeh, A., Klose, S., & Hartmann, D. H. 2004, ApJ, 609, 952
Zeh, A., Klose, S., & Kann, D. A. 2006, ApJ, 637, 889
Zhang, B., Fan, Y. Z., Dyks, J., Kobayashi, S., Mészáros, P., Burrows, D. N., Nousek, J. A., & Gehrels, N. 2006, ApJ, 642, 354
Zhang, B., & Mészáros, P. 2001, ApJ, 552, L35
Zhang, W., Woosley, S. E., & Heger, A. 2004, ApJ, 608, 365
Zhang, B., et al. 2009, ApJ, 703, 1696